Cancer Research

Three-Dimensional Culture of Mouse Renal Carcinoma Cells in Agarose Macrobeads Selects for a Subpopulation of Cells with Cancer Stem Cell or Cancer Progenitor Properties

Barry H. Smith[1,2,5], Lawrence S. Gazda[1,7], Bryan L. Conn[7], Kanti Jain[1,7], Shirin Asina[7], Daniel M. Levine[1,3], Thomas S. Parker[1,3], Melissa A. Laramore[7], Prithy C. Martis[7], Horatiu V. Vinerean[7], Eric M. David[1], Suizhen Qiu[1], Carlos Cordon-Cardo[6], Richard D. Hall[8], Bruce R. Gordon[1,2,4,5], Carolyn H. Diehl[1], Kurt H. Stenzel[1,2,3,4], and Albert L. Rubin[1,2,3,4]

Abstract

The culture of tumor cell lines in three-dimensional scaffolds is considered to more closely replicate the *in vivo* tumor microenvironment than the standard method of two-dimensional cell culture. We hypothesized that our method of encapsulating and maintaining viable and functional pancreatic islets in agarose–agarose macrobeads (diameter 6–8 mm) might provide a novel method for the culture of tumor cell lines. In this report we describe and characterize tumor colonies that form within macrobeads seeded with mouse renal adenocarcinoma cells. Approximately 1% of seeded tumor cells survive in the macrobead and over several months form discrete elliptical colonies appearing as tumor cell niches with increasing metabolic activity in parallel to colony size. The tumor colonies demonstrate ongoing cell turnover as shown by BrdU incorporation and activated caspase-3 and TUNEL staining. Genes upregulated in the tumor colonies of the macrobead are likely adaptations to this novel environment, as well as an amplification of G_1/S cell-cycle checkpoints. The data presented, including SCA-1 and Oct4 positivity and the upregulation of stem cell–like genes such as those associated with the Wnt pathway, support the notion that the macrobead selects for a subpopulation of cells with cancer stem cell or cancer progenitor properties. *Cancer Res; 71(3); 716–24. ©2011 AACR.*

Introduction

The *in vitro* investigation of cancer began with the report of the first human tumor cell line (HeLa) in 1952 (1). Use of this cell line has resulted in numerous advances in our understanding of cell and cancer biology which is largely attributable to its capacity to be easily cultured and grown in standard laboratory glassware or plasticware as 2-dimensional (2D) monolayers. Standard 2D cell culture, however, is limited in its ability to accurately recreate the *in vivo* tumor environment. The use of 3D culture systems are increasingly being employed to better mimic the *in vivo* tumor environment. Cells cultured in 3D systems are well organized with consistent shape and morphology and model cell–cell and cell–matrix interactions (2–5). Importantly, the use of 3D tumor cell culture has been shown to more accurately predict the *in vivo* response to cytotoxic therapy (6, 7).

As discussed by Fischbach and colleagues, the development of novel 3D tumor cell culture methods that recreate tumor niches would be a significant advance for the study of cancer biology (7). Ideally, such a system would enable expression of many of the distinguishing features of cancer as proposed by Hanahan and Weinberg, including unlimited cellular proliferative potential, self-sufficiency in growth signals, insensitivity to antigrowth signals, evasion of apoptosis, tissue invasion, and metastasis, and sustained angiogenesis as hallmarks of cancer (8). In addition, further characteristics defined over the last decade, such as the presence of cancer stem and/or progenitor cells and their hypothesized protective niches within tumors (9–16); the complex interactions between the local microenvironment and neoplastic cells, as well as between the tumor and the host, tumor internal heterogeneity/disorganization (17–26); and the characteristic, as well as diversity of tumor genomic patterns (27–29) should also be found in the 3D cultures.

We hypothesized that our method of encapsulating and maintaining viable and functional islets of Langerhans isolated from the pancreases of several species (30–33) might also provide a novel 3D method for the culture and investigation of tumor cell lines. In this report, we describe the successful

Authors' Affiliations: [1]The Rogosin Institute; Departments of [2]Surgery, [3]Biochemistry, and [4]Medicine, Weill Medical College of Cornell University; and [5]NewYork-Presbyterian Hospital; [6]Herbert Irving Cancer Center of Columbia University, New York, New York; [7]The Rogosin Institute-Xenia Division, Xenia, Ohio; and [8]Bob Evans Farms, Inc., Columbus, Ohio

Note: Supplementary data for this article are available at Cancer Research Online (http://cancerres.aacrjournals.org/).

This article is the first of two consecutive articles.

Corresponding Author: Barry H. Smith, The Rogosin Institute, 505 E. 70th St, HT-230, New York, NY 10021. Phone: 212-746-1551; Fax 212-288-8370. E-mail: bas2005@nyp.org.

doi: 10.1158/0008-5472.CAN-10-2254

encapsulation of tumor cells in 3D agarose–agarose macrobeads and show that these cancer macrobeads select for a population of tumor cells that form discrete colonies that gradually increase in size and metabolic activity. We have encapsulated diverse tumor cell lines from several species and have characterized in more detail the encapsulation of mouse renal adenocarcinoma cells (RENCA) in macrobeads. We demonstrate the ability of the cancer macrobeads to select cancer stem cell/progenitor cell–like cells and to provide a system suitable for the investigation of the natural history of tumorigenesis.

Materials and Methods

Cell lines

The RENCA tumor cell line used is a renal adenocarcinoma that arose spontaneously in Balb/c mice and was obtained from the National Cancer Institute (Bethesda, MD). RENCA cells were maintained *in vitro* (5% CO_2 + air at 37°C) in 75-cm^2 tissue culture flasks (BD Biosciences) containing RPMI 1640 medium (Invitrogen) with 10% neonatal calf serum (NCS; Invitrogen) with an initial seeding density of 1×10^6 cells per flask. Routine testing for *Mycoplasma* contamination has been consistently negative (Bionique Testing Laboratories, Inc.). Cell passages used were limited to no more than 20 from a frozen stock of these cells. When necessary to replenish such stocks, *in vivo* subcapsular renal passage was utilized to maintain stable tumor characteristics. MMT (mouse mammary tumor), K12 (feline mammary cancer), JEG-3 (human choriocarcinoma), DU145 (human prostate carcinoma), HCT 116 (human colorectal carcinoma), J82 (human urinary bladder transitional cell carcinoma), and MCF7 (human mammary gland adenocarcinoma) cell lines were originally obtained from the American Type Culture Collection (ATCC). ArCap10, a human prostate cancer cell line, was obtained from the University of Virginia at Charlottesville. All cell lines were maintained under equivalent culture and monitoring conditions as for the RENCA cell line.

RENCA macrobeads

For preparation of RENCA macrobeads, RENCA cells were seeded in 6-well plates (BD Biosciences) at 15,000 cells per well and grown for 5 days in 4 mL RPMI 1640 medium with 10% NCS per well until approximately 75% to 85% confluent. RENCA agarose–agarose macrobeads were prepared essentially as previously described for islet macrobeads (34). Briefly, 100 μL of 0.8% low-viscosity agarose (HSB-LV; Lonza Copenhagen ApS) was prepared in MEM (Sigma-Aldrich), maintained at 51°C to 53°C and mixed with 1.5×10^5 RENCA cells. The agarose cell suspension was immediately expelled into sterile mineral oil at room temperature using a sterile plastic transfer pipet to form the smooth semisolid core of the macrobead. Following the removal of mineral oil with RPMI-1640 media and overnight culture at 37°C in 5% CO_2 and air, the core was rolled in a sterile spoon that contained approximately 1 mL of 4.5% agarose in MEM maintained at 61°C to 63°C to apply a uniform outer coat of agarose. Before the outer coat of agarose solidified, the macrobead was transferred to mineral oil to form a smooth agarose–agarose macrobead and again washed with RPMI media prior to culture at 37°C in 5% CO_2 and air. For the other cell lines, the number of cells placed in the agarose matrix ranged from 100,000 to 250,000 cells. Macrobeads were cultured in 90-mm Petri dishes (Nunc) at 10 macrobeads per 40 mL of RPMI-1640 medium with 10% NCS. Medium was refreshed weekly. The metabolic properties of the macrobeads were evaluated using an MTT assay (Sigma-Aldrich).

Histology

Macrobeads were fixed in 10% neutral-buffered formalin overnight and transferred to PBS (Sigma-Aldrich) until processing, embedded in paraffin and 5-μm sections were stained with hematoxylin and eosin (Vector Laboratories; Polysciences; respectively; H&E). Formalin-fixed, paraffin-embedded macrobead sections were labeled with a biotin-conjugated mouse monoclonal antibody to PCNA (Invitrogen) or biotin-conjugated rabbit polyclonal antibody to active caspase-3 (BD Pharmingen) and detected with Alexa Fluor 658 conjugated streptavidin (Invitrogen); Apoptag peroxidase kit (Millipore) with VIP substrate (Vector Laboratories) counterstained with hematoxylin; FITC-conjugated mouse monoclonal antibody to BrdU (BD Biosciences); rabbit polyclonal antibody to p27 (Santa Cruz Biotechnology or Cell Signaling Technology) followed by a rhodamine (TRITC)-conjugated goat polyclonal antibody to rabbit IgG (Millipore); goat polyclonal antibody to SCA-1 (R&D Systems) followed by a TRITC-conjugated rabbit polyclonal antibody to goat IgG (Millipore); or rabbit polyclonal antibody to Oct4 (Abcam) followed by an Alexa Fluor 488–conjugated goat polyclonal antibody to rabbit IgG (Invitrogen). Nuclei were stained with 4′,6′-diamidino-2-phenylindole dihydrochloride (DAPI; Invitrogen).

Image acquisition

Monolayers were viewed with an inverted microscope (Axiovert S 100; Zeiss) and photographed (Axiocam MRc; Zeiss) at 100× magnification using MRGrab v1.1 software (Carl Zeiss Vision GmbH). Whole macrobeads were viewed with a dissecting microscope (model SZ6045; Olympus) with a bright-field illuminator base (model SZH-ILLD; Olympus) and photographed (Axiocam HRc, Zeiss) at 6× magnification using MRGrab v1.1 software. Macrobead sections stained with H&E were viewed with an inverted microscope (Axiovert S 100) using the bright field setting while fluorescence-labeled sections employed mercury vapor illumination (AttoArc 2; Atto Instruments) and photographed (Axiocam MRc) using MRGrab v1.1 software.

Isolation of RNA from RENCA macrobeads for Affymetrix analysis

Approximately 50 macrobeads between 9 and 12 months of age containing well-formed cellular colonies were harvested for RNA isolation on day 5 after medium change and placed in 125 mL of RNALater (Ambion) and stored at −20°C for future processing. Macrobeads were cut in half and the cell-containing cores were removed from the cell-free outer

agarose coat and placed in 15 mL (per 50 macrobeads) TRIzol reagent (Invitrogen). The macrobead cores in TRIzol were then homogenized with a Polytron PT 1200 C homogenizer (Kinematica), aliquoted to 1.5-mL microfuge tubes and incubated at 30°C for 5 minutes before the addition of 200 μL of chloroform. The tubes were shaken vigorously and incubated at 30°C for an additional 3 minutes. Samples were centrifuged at 13,000 rcf for 15 minutes at 4°C in a microcentrifuge (model 5417R; Eppendorf). RNA was precipitated from supernatants with the addition of 500 μL of isopropanol, followed by a short vortex and 10 minutes room temperature incubation. The precipitate was pelleted at 13,000 rcf at 4°C for 10 minutes and the pellets were washed twice with 1 mL of 70% ethanol to remove salts. The pellets were dried and resuspended in water.

Isolation of RNA from RENCA monolayers

RENCA monolayers were routinely maintained in RPMI 1640 medium supplemented with 10% NCS. For mRNA, trypsinized RENCA cells were seeded at 20,000 cells per 40-mm well (6-well plate) in 4 mL of medium. Medium was replenished on day 2 and cells were harvested on day 4 in late log growth. Cells were washed with 2 mL cold PBS (without Ca^{2+} or Mg^{2+}). Total RNA was prepared using the RNeasy Mini Kit (Qiagen).

Gene microarrays and data analysis by GenMapp and MAPPFinder gene microarrays

RNA quality was confirmed with Total RNA Nano chips (Bio Sizing Lab-on-Chip) on the Bioanalyzer 2100 (Agilent Technologies). Samples of total RNA meeting criteria (rRNA > 30% of area, 28s/18s ratio > 1.5) were used for reverse transcription to cDNA. The standard target labeling assay (1–15 μg total RNA) was followed as per the Affymetrix Gene Chip Expression Analysis Technical Manual 1999. Biotin-labeled cRNA was then synthesized using the BioArray HighYield RNA transcript labeling kit (Affymetrix), purified by RNeasy Mini Kit (Qiagen), fragmented to a mean size of 35 to 200 base pairs and then evaluated for quality by hybridization to Test 3 Chip (Affymetrix). Samples with background between 30 and 100, and scale factor between 1 and 5 were hybridized to Affymetrix Mu94v2 A, B, and C chips in that order. All chips were scanned at the Genomics Resource Center of The Rockefeller University as per the Affymetrix Gene Chip Expression Analysis Technical Manual 1999.

Analysis of gene expression data

The data set included 3 biological replicate samples each from RENCA macrobeads and RENCA cell monolayers. Average probe intensities were globally scaled to a target intensity of 250. All data were normalized at the probe-level by GC-RMA using GeneTraffic software version 3.1.2. Data within each chip type (A, B, or C) were normalized separately and then combined in a single Excel worksheet. Fold change was calculated as $\log_2$(macrobead/monolayer). ANOVA *P* values were calculated for expression intensity from the 3 values of macrobead and monolayer expression of each probe.

GenMapp and MAPPFinder

GenMapp 2.1.0 and MAPPFinder 2.0 software packages (www.GenMapp.org) were used to identify the global patterns of changes in gene expression of cells within macrobeads. All probe sets measured in the experiment were used as input to GenMAPP. Gene Ontology (GO) annotations were based on the GenMAPP Mm-Std_20051114.gdb database. The GenMAPP Criteria Builder was used to filter the data using the following criteria: ANOVA greater than 0.10, signal intensity of macrobead sample greater than100, $\log_2 R$ greater than 0.20 for upregulated genes and $\log_2 R$ greater than −0.20 for downregulated genes. These criteria selected 1,313 distinct upregulated genes and 493 distinct downregulated genes. The adjusted (for multiple comparisons) permuted *P* value from MAPPFinder was used to select significant GO terms ($P < 0.05$).

RT^2 profiler pathway focused PCR array, RNA isolation, and stem cell PCR array

Total RNA from 3 biological replicates of RENCA monolayer cells and RENCA macrobeads (ages: 1, 12, and 36 weeks) was isolated using an RNeasy mini kit followed by genomic DNA elimination with an RNase-Free DNase Set (Qiagen), according to the manufacturer's recommendations. RNA (2 μg) was reverse transcribed using the RT^2 First Strand Kit (SABiosciences). Synthesized cDNA (18 ng) was added to each well of the mouse stem cell RT^2 Profiler PCR array (SABiosciences) to analyze the expression levels of 84 genes implicated in maintaining stem cells in a differentiated or undifferentiated state. Quantitative real-time PCR reactions were performed using RT^2 Real-Time SYBR Green PCR Master Mix (SABiosciences) in a DNA Engine Opticon 2 real-time PCR machine (MJ Research), according to the manufacturer's instructions.

Data normalization and analysis

The threshold cycle number (Ct) for each PCR reaction was determined by setting the same threshold value across all PCR arrays. The relative amount of transcripts for each gene in every sample type was normalized to the average of the housekeeping (HKG) genes (Gusb, Hprt1, Hsp90ab1, Gapdh, and Actb) and calculated as follows: ΔCt is the $\log_2$ difference between the gene and the HKG gene, and is obtained by subtracting the average Ct of HKG from the Ct value of the gene on a per-array basis. A list of differentially expressed genes was identified by using the cutoff criteria of a *P* value less than 0.05 as assessed by an unpaired *t* test with a mean difference of 2-fold or greater.

Results

The formation of viable and metabolically active tumor colonies within the macrobead

To test the hypothesis that neoplastic cells entrapped in an agarose matrix would survive during *in vitro* culture, mouse renal adenocarcinoma (RENCA), feline breast carcinoma (K12), as well as human breast (MCF7), prostate (ArCap10 and DU145), bladder (J82), colon (HCT116) and choriocarcinoma (JEG-3) cell lines were all successfully encapsulated and maintained in 6- to 8-mm diameter agarose–agarose

macrobeads, albeit with various growth rates and tumor colony formation competence. For example, the ranking of the encapsulated human tumor cell lines as to the highest metabolic activity (a reflection of colony formation within the macrobead) was J82 > MCF7 > HCT116 > DU145 with mean MTT values at 4 weeks of 1.299 ± 0.01, 1.282 ± 0.066, 0.508 ± 0.026, and 0.395 ± 0.175 OD, respectively. The RENCA cell line proved to be easily cultured and consistently formed tumor colonies within the macrobeads and was thus selected for more in-depth study.

Figure 1A is a micrograph of RENCA cells under 2D culture conditions on day 5 postpassage showing the epithelioid morphology when grown in monolayer culture. When encapsulated and cultured in agarose–agarose macrobeads, RENCA cells form discrete tumor colonies over time (Fig. 1B). Encapsulated RENCA cells are metabolically active 1 day after encapsulation as shown during an MTT assay in Figure 1B. A photomicrograph of an H&E-stained macrobead section 1 day after encapsulation also demonstrates the viability of the encapsulated cells (Fig. 1B; day 1).

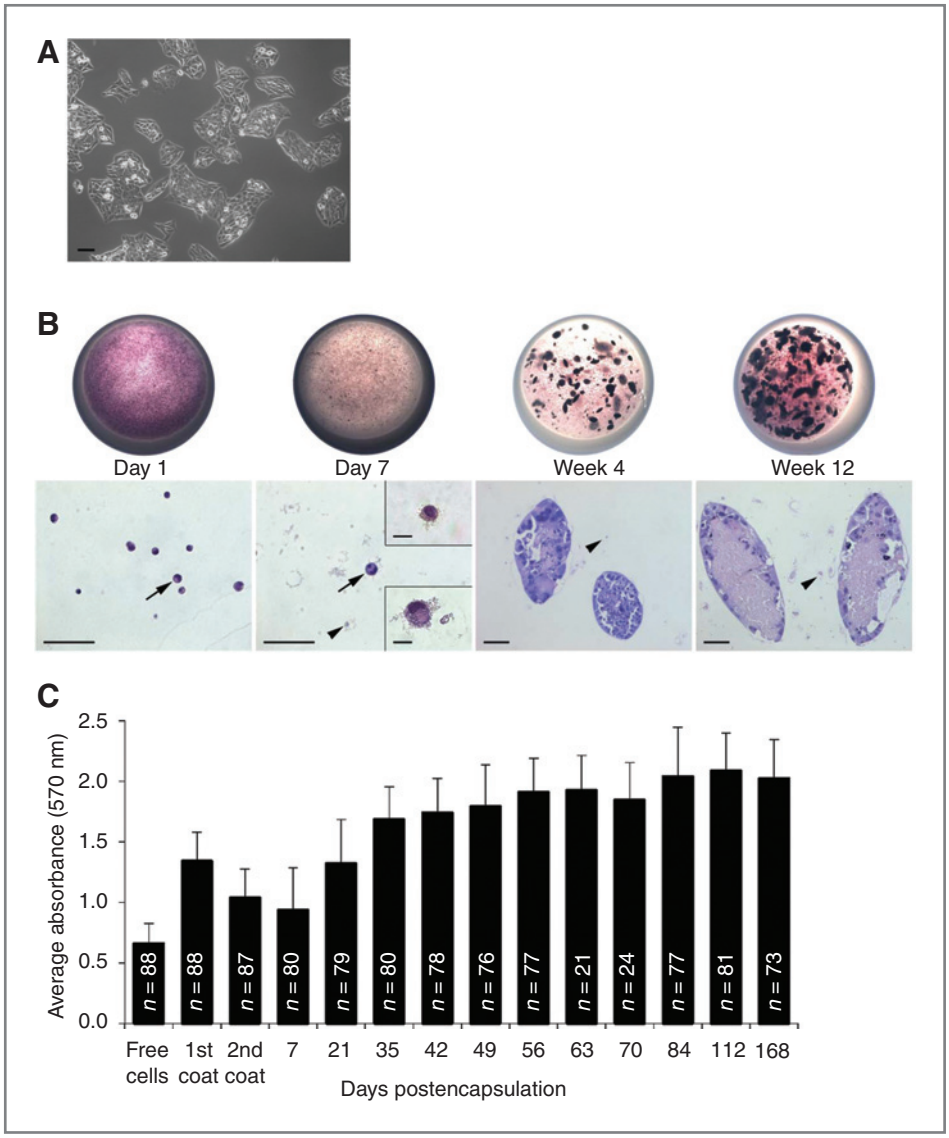

Figure 1. Natural history of the RENCA macrobead. A, 100× phase-contrast image of RENCA cells at day 5 of monolayer culture. Scale bar, 50 μm. B, typical macroscopic and microscopic appearances of day 1 through week 12 RENCA macrobeads. Top, macroscopic photographs of the RENCA macrobeads were taken during an MTT assay and demonstrate metabolically active cells and colonies (purple color) on day 1, week 4, and week 12 with a significant loss of metabolically active cells on day 7. Each macrobead has a diameter of 6 to 8 mm. Bottom, micrographs of H&E-stained sections of RENCA macrobeads demonstrating the significant loss of day 1 encapsulated viable cells by day 7 in which 2 distinct types of cells survive (insets day 7) that produce ellipsoid tumor colonies that enlarge over time reaching a final size around 12 weeks of age. Arrows point to viable cells and arrowheads point to cell debris from dead cells. Scale bars for larger micrographs are 50 μm. Scale bars for insets at day 7 are 10 μm. C, average absorbance of RENCA macrobeads over time demonstrating increasing metabolic activity with increasing colony size.

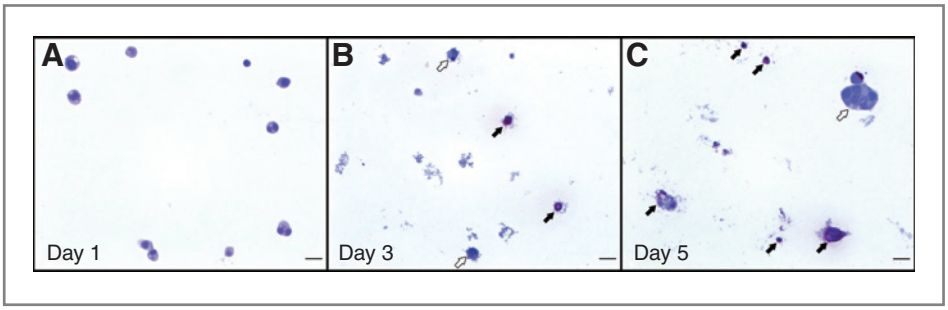

Figure 2. TUNEL staining for apoptosis of recently encapsulated RENCA cells. A, 1 day after encapsulation, all cells are TUNEL negative. B, by day 3 postencapsulation, approximately 50% of cells exhibit TUNEL-positive staining. Some cell debris is now visible. C, approximately 99% of encapsulated RENCA cells are TUNEL positive by day 5. A small tumor colony has started to form (top right corner). White arrows point to TUNEL-negative cells, whereas black arrows point to TUNEL-positive cells. Scale bars, 20 μm.

Irrespective of the optimal number of cells encapsulated for each of the lines, the cell lines of various tumors all undergo similar changes over time in the macrobead. Within 3 to 10 days of being placed in the macrobeads, an estimated 99% of the cells undergo an apoptotic cell death (Fig. 2). A remarkable loss of cell viability and metabolic activity is observed 1 week postencapsulation (Fig. 1B; day 7). The morphology of the surviving cells is markedly different from that of RENCA cells in monolayer. The surviving cells in the macrobead are of at least 2 types: (1) large and irregular with a high cytoplasm-to-nuclear ratio and (2) small and round with a much lower ratio of cytoplasmic-to-nuclear volume (Fig. 1B; day 7 inset) compared with the epithelioid-shaped cells observed in monolayer (Fig. 1A).

Over the next several weeks, the very small numbers of cells remaining in the agarose (in the case of the RENCA line, an estimated 1,500 cells), form ellipsoid-shaped colonies. At 4 weeks of age young RENCA macrobeads exhibit the presence of small metabolically active and viable tumor colonies within the first layer of agarose (Fig. 1B, 4 weeks). By 12 weeks of age, older RENCA macrobeads reveal the presence of larger, metabolically active and viable tumor colonies (Fig. 1B, 12 weeks). The colonies in older macrobeads form an external layer, 1 to 2 cells deep with a dense eosinophilic cell-free area at the center of the colony.

As the RENCA macrobeads mature and larger tumor colonies form, the metabolic activity increases accordingly (Fig. 1C). Other tumor cell lines are also able to be maintained in the environment of the macrobead and demonstrate similar growth characteristics. For example, human cell lines derived from bladder, prostate, colon, and breast tumors all form metabolically active and viable tumor colonies within the agarose–agarose macrobead (Supplementary Fig. S1).

The colonies within the macrobeads can be maintained in culture indefinitely (at least 3 years for RENCA macrobeads) with little increase in total cell number or colony volume. Released from the agarose environment after 3 years, the RENCA cells from the colonies retain their neoplastic cell properties, both with respect to their *in vitro* proliferation and their ability to form tumors *in vivo* in Balb/c mice. Suspensions of single, nonneoplastic fibroblasts and hepatocytes do not form colonies in the agarose macrobead (data not shown).

Tumor colonies are maintained by continual cellular proliferation and apoptosis

Although the colony size is stable over years of culture in the macrobeads, individual cells are clearly turning over. Cell nuclei stain positively for proliferating cell nuclear antigen (PCNA, Fig. 2A), Ki67 (not shown), and actively incorporate BrdU (Fig. 2B). A population of cells within the colony exhibit nuclear localization of p27 (Fig. 2C). In addition, the cells stain positively for activated caspase-3 (Fig. 2D) and are TUNEL-positive (data not shown), suggesting that cell proliferation is offset by apoptosis.

Gene expression of RENCA macrobeads

To further characterize the nature of the cell colonies that survive in the RENCA macrobeads, we have compared gene expression in 6-month-old macrobeads with late log-phase RENCA monolayer cells. GenMAPP and MAPPFinder were used to identify large groups of responding genes according to Gene Ontology (GO) groupings. The genomic results parallel many of the histological observations. There was a broad reduction within the macrobeads of gene expression coding for cytoplasmic, ribosomal, mitochondrial, and nuclear proteins involved in RNA splicing and processing (Supplementary Table 1). The upregulated GO categories included endoplasmic stress, unfolded protein response and lysosomal proteins that may be adaptations to the environment, reflecting the need to process agarose, matrix proteins, and debris trapped within the macrobead (Supplementary Table 1).

The expression of many genes that code for adhesion proteins or extracellular (secreted) proteins changed in the macrobeads. Seventeen of the top 20 upregulated probes were secreted matrix proteins or cell-surface proteins interacting with the extracellular matrix (Supplementary Table 2). Among these were Bglap1/osteocalcin and Mmp10/stromelysin 2 that are very likely produced as adaptations to the macrobead microenvironment. A number of genes involved in regulating angiogenesis including, VEGF-B, SLIPI, thrombospondin, Mmp13, and cathepsins B and D were also upregulated. The 2 most downregulated genes, high molecular weight tropomyosin and cytohesin binding protein, permit anchorage-independent growth when downregulated (Supplementary Table 3). Many genes that function in mitosis were also

downregulated as a group (Supplementary Table 4). On balance, it appears that the preponderance of gene changes in the cells within the macrobead are adaptations to the environment or relate to strengthening of the G_1/S cell-cycle checkpoints.

Macrobeads select for cancer stem cell/progenitor cell–like populations

Given the aforementioned observations that the majority of initially encapsulated cells die off and that discrete colonies form with continual cell renewal, we investigated the possibility that the macrobeads possessed the capacity to select for a population of cells with cancer stem cell/progenitor cell–like attributes.

Immunofluorescence studies show that the environment within the macrobead selects for a subpopulation of large cells expressing tumor stem or progenitor cell markers along with at least one other subpopulation of smaller cells. In the case of the RENCA cell line, the stem cell–associated markers include CD44(CD24$^-$), stem cell antigen-1 (SCA-1), and Oct4 but not CD133 (not shown; Fig. 3). In addition, a number of genes in the canonical Wnt signaling pathway are significantly upregulated, as are stem cell markers downstream of Wnt, including SCA-1 (10-fold up), CD44 (4-fold up), and ABC White 2 (side population marker: 1.8-fold up; Supplementary Table 4). β-Catenin, which is downstream of SCA-1 in the canonical Wnt signaling pathway, can also be detected (Supplementary Table 4). Although the gene expression results for SCA-1 indicate a 10-fold enrichment of progenitor cells (Supplementary Table 4), the immunofluorescence data show that SCA-1 positive cells are still a minority (Fig. 3).

To investigate stem cell/progenitor cell–like gene expression in the RENCA macrobeads at various times of colony

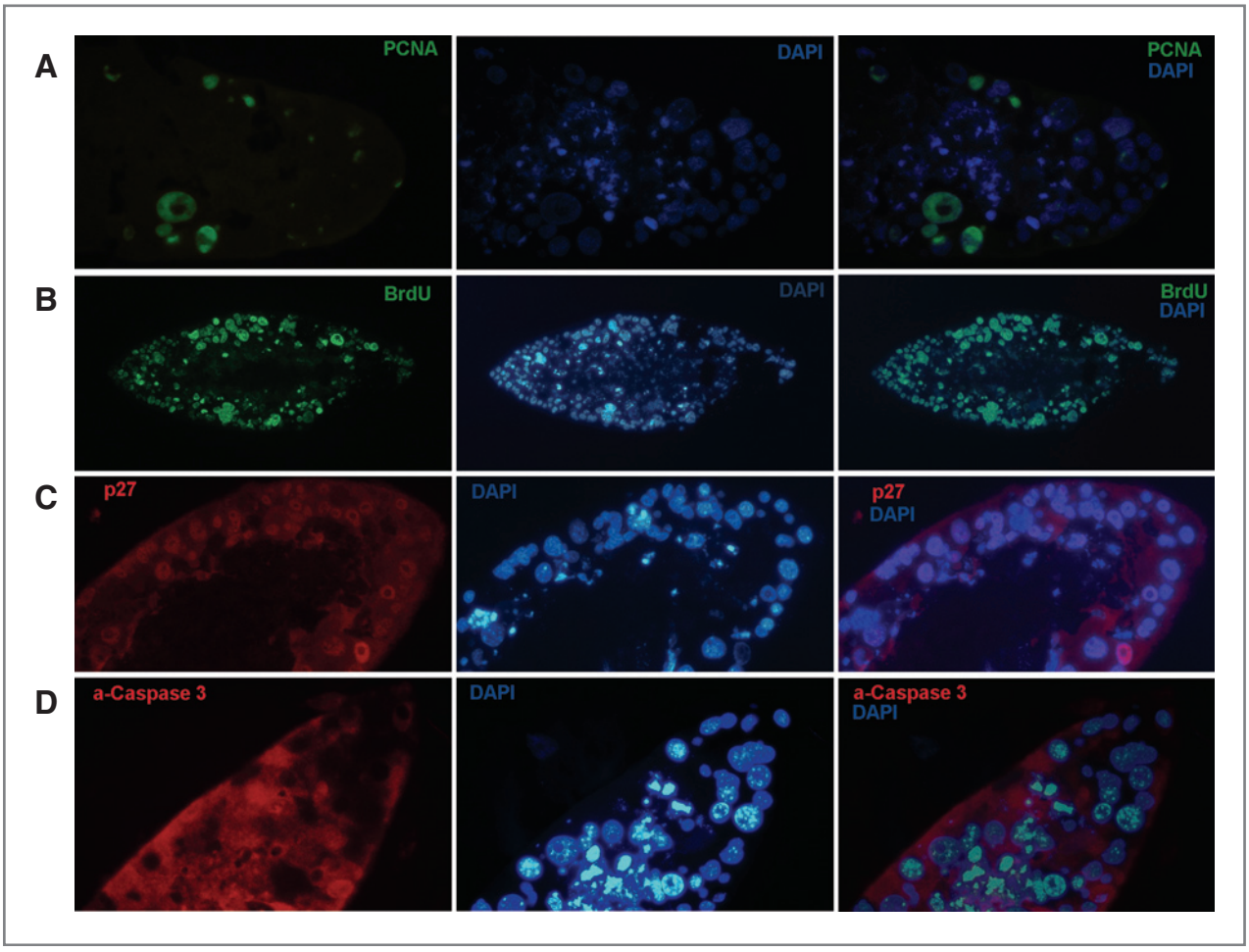

Figure 3. Immunofluorescent staining for selected proliferation and apoptosis markers expressed in macrobeads. A, PCNA staining (green) of RENCA macrobead colonies shows that a significant population of cells is actively dividing. B, typical micrograph after BrdU labeling (3-day pulse, 8-day recovery) of mature macrobeads demonstrating significant cellular proliferation within RENCA colonies. C, Pan-p27 staining (red) reveals an absence of nuclear p27 localization in certain cells, whereas other cells show clear nuclear localization. This is consistent with the pattern of PCNA staining because the proliferating cells are likely to be p27 negative whereas the p27-positive cells are more likely to be quiescent. D, activated caspase-3 (red) is generally present in cell cytoplasm and extracellularly (from previously apoptosed cells). Taken together, the PCNA/BrdU/p27/a-casp-3 data suggest that colony homeostasis is achieved through a balance of cell proliferation, arrest, and death.

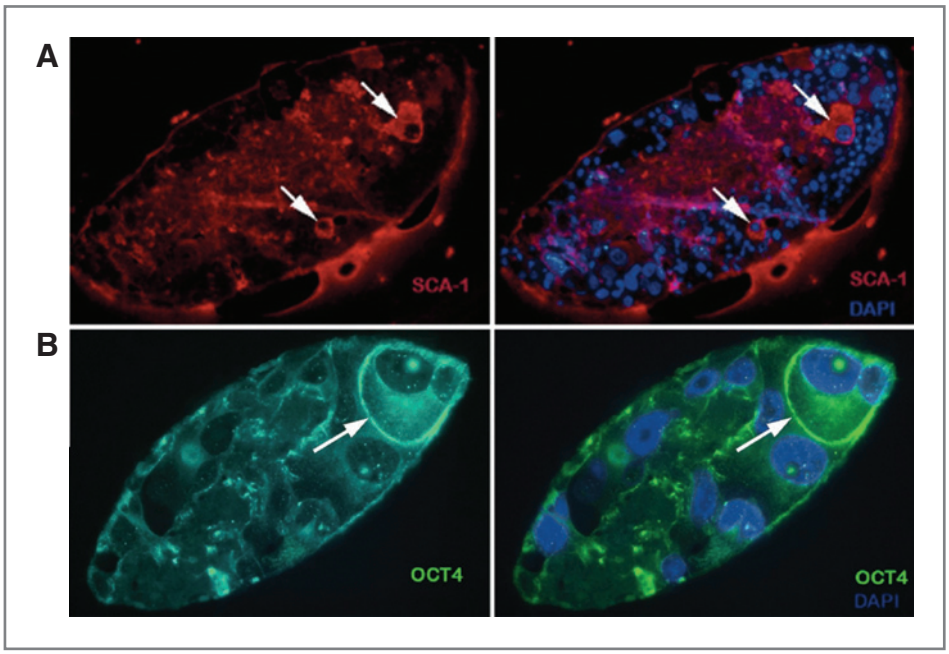

Figure 4. Immunofluorescent staining for stem cell–associated markers. A, the cell surface protein SCA-1 (red) is found throughout macrobead colonies, as well as in the surrounding agarose matrix. Rare discrete cells are also SCA-1 positive (arrows). B, a minority of cells within individual RENCA colonies express the Oct4 protein (arrow).

development, we performed focused PCR array assays on macrobeads at 1 week, 12 weeks, and 36 weeks of age, and compared the gene expression with RENCA monolayers. As shown in Figure 4 several genes previously identified from the Affymetrix studies were again found to be upregulated in older macrobeads as compared with RENCA monolayer cells (e.g., CD44 and Wnt1). Interestingly, both CD44 and Wnt1 displayed a higher level of gene expression in macrobeads that were only 1 week old as compared with older macrobeads. Osteocalcin mRNA and cadherin 1 mRNA were significantly increased in both 12- and 36-week-old macrobeads, as was the expression of aldehyde dehydrogenase 1A1 and aldehyde dehydrogenase 2 (Figs. 4 and 5).

Discussion

Cells derived from epithelial tumors encapsulated in agarose–agarose macrobeads undergo a process that results in a selection of at least 2 subpopulations of cells. One such population of cells has properties of stem cells and appears, on the basis of our data to date, to share similarities with the tumor stem, progenitor, or founder cells reported in the literature for breast, colon, and glial-derived tumors (11–13, 35, 36), although the mouse kidney cancer cells that we have utilized in the majority of our macrobead studies are not positive for CD133.

We are continuing to define the extent to which these cells are indeed progenitor or stem cells responsible for the production of *in vivo* tumors and have several lines of evidence indicating this is the case. First, as already noted, the tumor cells that survive and form colonies in the macrobead exhibit stem cell markers (in the case of RENCA, $CD44^+/CD24^-$, $SCA\text{-}1^+$, and $Oct4^+$) similar or parallel to those already described for other solid tumors (11–13, 35–43). Second, analysis of gene microarray data from the cells in the macrobeads indicate that pathways which have been associated with stem cells, such as the Wnt pathway, are enhanced compared with the same gene pathways in the total population of RENCA cells in monolayer culture. Third, the surviving 1% or less of the 150,000 RENCA cells originally placed in the agarose matrix of the macrobead are fully capable of restoring the total tumor cell population *in vitro* and *in vivo* when released from the macrobead after long periods of up to at least 3 years in culture. In other words, it is only a small subfraction of the total population that has such capability. It is these cells that selectively survive and form stable colonies in the macrobead, while retaining the ability to proliferate in monolayer culture and form tumors *in vivo*.

The colonies that form in the macrobeads are themselves of interest because it appears that they may represent a form of a cancer stem cell niche. If this is so, the cancer macrobead presents a way to create or recreate such bodies in isolation and thereby study them and their cellular subpopulations and the molecular biology of the interactions between the stem cells and other cell types. The macrobeads can thus be a test vehicle for current therapeutic agents and the development of new approaches. In fact, our present efforts are aimed at better defining the gene pathways that are active in the subpopulations of cells that form the colonies found in the macrobeads.

It is evident from the studies reported here that the colonies are active cell populations exhibiting both proliferation and apoptosis, with an equilibrium between the two being achieved because the colony size eventually stabilizes. The cells in the colonies consist of at least two populations, that is, tose larger cells exhibiting stem cell markers, and smaller actively proliferating cells not displaying stem cell markers.

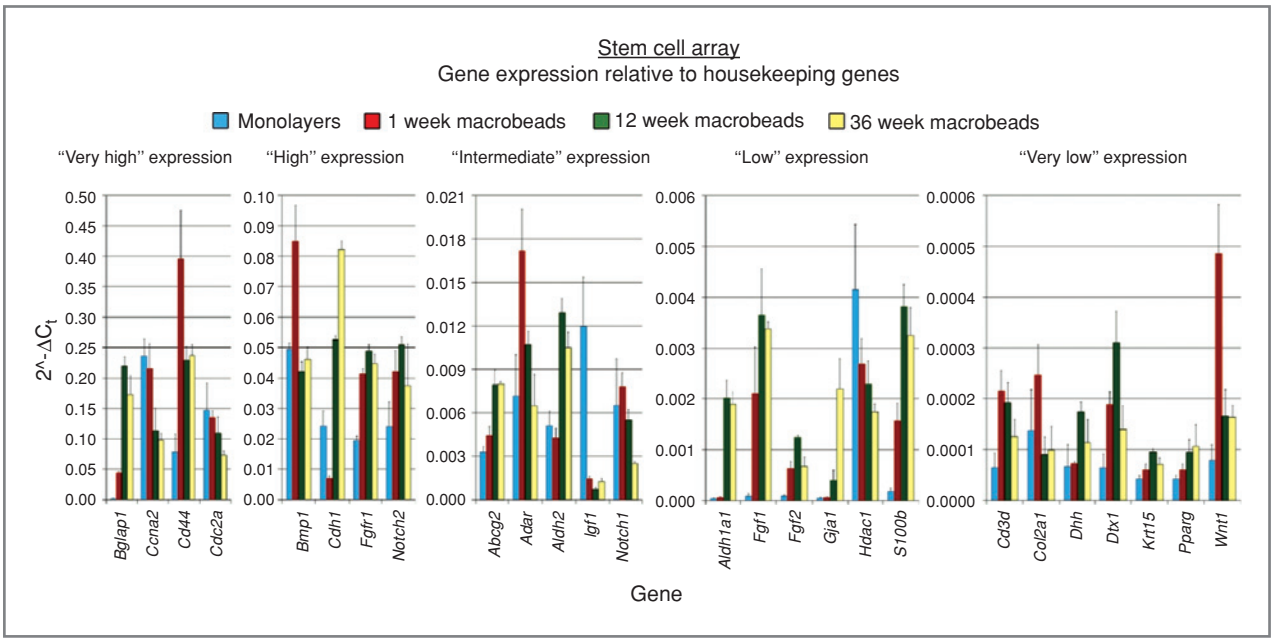

Figure 5. Real-time RT-PCR of RENCA monolayers and macrobeads. Total RNA was extracted from RENCA monolayers and macrobeads of ages 1, 12, and 36 weeks. Stem Cell PCR Array (SABiosciences) was used to simultaneously examine the expression levels of 84 genes. Data was normalized to average levels of 5 housekeeping genes (*Gusb*, *Hprt1*, *Hsp90ab1*, *Gapdh*, and *Actb*) and expressed as fold change in RNA calculated by using the $2^{-\Delta Ct}$ method. The figure shows only the differentially regulated genes defined by the cutoff criteria of a *P* value less than 0.05 as assessed by an unpaired *t* test with a mean difference 2-fold or greater.

Repeated gene microarray studies show that the gene activity profile of the cells within the macrobead is stable and reproducible, as well as distinct from that exhibited by RENCA cells in monolayer culture.

The agarose cancer macrobead described in this report offers numerous advantages over previously published 3D tumor culture systems. The agarose, although a biological material derived from seaweed, is highly purified, and we have found all Lots of agarose used to date ($n = 3$) for the production of RENCA macrobeads to support RENCA cell growth suggesting little Lot-to-Lot variability in this raw material. In fact, the 2 most recent Lots of agarose used for the production of RENCA macrobeads in the last 3 years have resulted in MTT values of 1.264 ± 0.348 OD and 1.320 ± 0.290 OD at 5 weeks postencapsulation.

In addition, multiple tumor cell types are able to grow in this newly described 3D culture system, allowing for the study of various cancer types. Given the ability to culture different types of tumor cells, it is possible that other cell types may also be successfully co-encapsulated to more precisely replicate the natural tumor environment. The cancer macrobeads are easily adapted to the use of standard laboratory techniques including the ability to perform immunohistochemistry, the ability to isolate RNA, and the ability to test small molecule signaling and tumor inhibitors on the 3D colonies. A significant advantage of this 3D tumor culture method is the avoidance of issues related to the xenotransplantation of tumor cells such as species-specific growth factors and nonsupportive transplantation sites. Long-term culture is possible, allowing the study of cancer colonies over months and even years, as well as the possibility of studying the very early events in tumor development and growth.

In summary, on the basis of these findings, we believe that the cancer macrobeads offer a unique opportunity to study the molecular biological basis of tumor biology, in part by virtue of their ability to select a subpopulation of cells that appear to have stem cell properties and to be responsible for enabling the founding and perpetuation of tumors. In addition, of course, the macrobeads provide a ready means for the *in vitro* preclinical testing of proposed therapeutic agents that, to be optimally effective, must show activity against such cells.

Disclosure of Potential Conflicts of Interests

No potential conflicts of interests were disclosed.

Acknowledgments

The authors acknowledge the invaluable assistance of Bob Evans Farms, Inc., in enabling this work, as well as that of Brian Doll, Deborah Hoffer, Allison Beyer, Madeline Wiles, and their colleagues at the Xenia Division of The Rogosin Institute and Rimma Belenkaya for superb technical assistance.

Grant Support

This work was financially supported by Metromedia Bio-Science, LLC.

The costs of publication of this article were defrayed in part by the payment of page charges. This article must therefore be hereby marked *advertisement* in accordance with 18 U.S.C. Section 1734 solely to indicate this fact.

Received June 22, 2010; revised September 24, 2010; accepted October 13, 2010; published OnlineFirst January 25, 2011.

References

1. Gey G, Coffman W, Kubicek M. Tissue culture studies of the proliferative capacity of cervical carcinoma and normal epithelium. Cancer Res 1952;12:364–5.
2. Sutherland RM. Cell and environment interactions in tumor microregions: the multicell spheroid model. Science 1988;240:177–84.
3. Kim JB. Three-dimensional tissue culture models in cancer biology. Semin Cancer Biol 2005;15:365–77.
4. Hebner C, Weaver VM, Debnath J. Modeling morphogenesis and oncogenesis in three-dimensional breast epithelial cultures. Annu Rev Pathol 2008;3:313–39.
5. Yamada KM, Cukierman E. Modeling tissue morphogenesis and cancer in 3D. Cell 2007;130:601–10.
6. dit Faute MA, Laurent L, Ploton D, Poupon MF, Jardillier JC, Bobichon H. Distinctive alterations of invasiveness, drug resistance and cell-cell organization in 3D-cultures of MCF-7, a human breast cancer cell line, and its multidrug resistant variant. Clin Exp Metastasis 2002;19:161–8.
7. Fischbach C, Chen R, Matsumoto T, Schmelzle T, Brugge JS, Polverini PJ, et al. Engineering tumors with 3D scaffolds. Nat Methods 2007;4:855–60.
8. Hanahan D, Weinberg RA. The hallmarks of cancer. Cell 2000;100:57–70.
9. Reya T, Morrison SJ, Clarke MF, Weissman IL. Stem cells, cancer, and cancer stem cells. Nature 2001;414:105–11.
10. Al-Hajj M, Wicha MS, Benito-Hernandez A, Morrison SJ, Clarke MF. Prospective identification of tumorigenic breast cancer cells. Proc Natl Acad Sci U S A 2003;100:3983–8.
11. SK, Clarke ID, Terasaki M, Bonn VE, Hawkins C, Squire J, et al. Identification of a cancer stem cell in human brain tumors. Cancer Res 2003;63:5821–8.
12. Liu G, Yuan X, Zeng Z, Tunici P, Ng H, Abdulkadir IR, et al. Analysis of gene expression and chemoresistance of CD133+ cancer stem cells in glioblastoma. Mol Cancer 2006;5:67.
13. O'Brien CA, Pollett A, Gallinger S, Dick JE. A human colon cancer cell capable of initiating tumour growth in immunodeficient mice. Nature 2007;445:106–10.
14. Boman BM, Wicha MS. Cancer stem cells: a step toward the cure. J Clin Oncol 2008;26:2795–9.
15. Visvader JE, Lindeman GJ. Cancer stem cells in solid tumours: accumulating evidence and unresolved questions. Nat Rev Cancer 2008;8:755–68.
16. Welm BE, Tepera SB, Venezia T, Graubert TA, Rosen JM, Goodell MA. Sca-1(pos) cells in the mouse mammary gland represent an enriched progenitor cell population. Dev Biol 2002;245:42–56.
17. Shekhar MPV, Pauley R, Heppner G. Extracellular matrix-stromal cell contribution to neoplastic phenotype of epithelial cells in the breast. Breast Cancer Res 2003;5:130–5.
18. Anderson AR, Weaver AM, Cummings PT, Quaranta V. Tumor morphology and phenotypic evolution driven by selective pressure from the microenvironment. Cell 2006;127:905–15.
19. Yang L, Moses HL. Transforming growth factor beta: tumor suppressor or promoter? Are host immune cells the answer? Cancer Res 2008;68:9107–11.
20 Cheng N, Chytil A, Shyr Y, Joly A, Moses HL. Transforming growth factor-beta signaling-deficient fibroblasts enhance hepatocyte growth factor signaling in mammary carcinoma cells to promote scattering and invasion. Mol Cancer Res 2008;6:1521–33.
21. Joyce JA, Baruch A, Chehade K, Meyer-Morse N, Giraudo E, Tsai FY, et al. Cathepsin cysteine proteases are effectors of invasive growth and angiogenesis during multistage tumorigenesis. Cancer Cell 2004;5:443–53.
22. Sinnamon MJ, Carter KJ, Fingleton B, Matrisian LM. Matrix metalloproteinase-9 contributes to intestinal tumourigenesis in the adenomatous polyposis coli multiple intestinal neoplasia mouse. Int J Exp Pathol 2008;89:466–75.
23. Polyak K, Weinberg RA. Transitions between epithelial and mesenchymal states: acquisition of malignant and stem cell traits. Nat Rev Cancer 2009;9:265–73.
24. van Rheenen J, Condeelis J, Glogauer M. A common cofilin activity cycle in invasive tumor cells and inflammatory cells. J Cell Sci 2009;122:305–11.
25. Robinson BD, Sica GL, Liu YF, Rohan TE, Gertler FB, Condeelis JS, et al. Tumor microenvironment of metastasis in human breast carcinoma: a potential prognostic marker linked to hematogenous dissemination. Clin Cancer Res 2009;15:2433–41.
26. Schreiber H. Tumor-specific immune responses. Semin Immunol 2008;20:265–6.
27. Andre F, Job B, Dessen P, Tordai A, Michiels S, Liedtke C, et al. Molecular characterization of breast cancer with high-resolution oligonucleotide comparative genomic hybridization array. Clin Cancer Res 2009;15:441–51.
28. Nakao K, Mehta KR, Fridlyand J, Moore DH, Jain AN, Lafuente A, et al. High-resolution analysis of DNA copy number alterations in colorectal cancer by array-based comparative genomic hybridization. Carcinogenesis 2004;25:1345–57.
29. Witte JS. Prostate cancer genomics: towards a new understanding. Nat Rev Genet 2009;10:77–82.
30. Jain K, Cai BR, Patel S, Yang H, Smith BH, Suthanthiran M, Rubin AL, et al. Consistent long-term allograft survival in murine pancreatic islet transplants without immunosuppression. Transplant Proc 1994;26:3492–3.
31. Jain K, Yang H, Asina SK, Patel SG, Desai J, Diehl C, et al. Long-term preservation of islets of Langerhans in hydrophilic macrobeads. Transplantation 1996;61:532–6.
32. Jain K, Asina S, Yang H, Blount ED, Smith BH, Diehl CH, et al. Glucose control and long-term survival in biobreeding/Worcester rats after intraperitoneal implantation of hydrophilic macrobeads containing porcine islets without immunosuppression. Transplantation 1999;68:1693–1700.
33. Gazda LS, Adkins H, Bailie JA, Byrd W, Circle L, Conn B, et al. The use of pancreas biopsy scoring provides reliable porcine islet yields while encapsulation permits the determination of microbiological safety. Cell Transplant 2005;14:427–39.
34. Jain K, Yang H, Cai BR, Hauque B, Hurvitz AI, Diehl C, et al. Retrievable, replaceable, macroencapsulated pancreatic islet xenografts. Long-term engraftment without immunosuppression. Transplantation 1995;59:319–24.
35. Ricci-Vitiani L, Lombardi DG, Pilozzi E, Biffoni M, Todaro M, Peschle C, et al. Identification and expansion of human colon-cancer-initiating cells. Nature 2007;445:111–5.
36. Zucchi I, Sanzone S, Astigiano S, Pelucchi P, Scotti M, Valsecchi V, et al. The properties of a mammary gland cancer stem cell. Proc Natl Acad Sci U S A 2007;104:10476–81.
37. Li Y, Welm B, Podsypanina K, Huang S, Chamorro M, Zhang X, et al. Evidence that transgenes encoding components of the Wnt signaling pathway preferentially induce mammary cancers from progenitor cells. Proc Natl Acad Sci U S A 2003;100:15853–8.
38. Ponti D, Costa A, Zaffaroni N, Pratesi G, Petrangolini G, Coradini D, et al. Isolation and in vitro propagation of tumorigenic breast cancer cells with stem/progenitor cell properties. Cancer Res 2005;65:5506–11.
39. Xin L, Lawson DA, Witte ON. The Sca-1 cell surface marker enriches for a prostate-regenerating cell subpopulation that can initiate prostate tumorigenesis. Proc Natl Acad Sci U S A 2005;102:6942–7.
40. Cheng L, Sung MT, Cossu-Rocca P, Jones TD, MacLennan GT, De Jong J, et al. OCT4: biological functions and clinical applications as a marker of germ cell neoplasia. J Pathol 2007;211:1–9.
41. Holmes C, Stanford WL. Concise review: stem cell antigen-1: expression, function, and enigma. Stem Cells 2007;25:1339–47.
42. Nakshatri H, Srour EF, Badve S. Breast cancer stem cells and intrinsic subtypes: controversies rage on. Curr Stem Cell Res Ther 2009;4:50–60.
43. Xu Y, Stamenkovic I, Yu Q. CD44 attenuates activation of the hippo signaling pathway and is a prime therapeutic target for glioblastoma. Cancer Res 2010;70:2455–64.